Mode Propagation Analysis of Magnetically Biased Graphene Microstrips via an Efficient Finite-Difference Scheme

Stamatios Amanatiadis[1], Tadao Ohtani[2], Theodoros Zygiridis[3], Yasushi Kanai[4], and Nikolaos Kantartzis[1]

[1]Department of Electrical and Computer Engineering, Aristotle University of Thessaloniki, 54124 Thessaloniki, Greece
[2]1-17-134 Omachi, Asahikawa 070-0841, Japan
[3]Department of Electrical and Computer Engineering, University of Western Macedonia, 50131 Kozani, Greece
[4]Department of Information and Electronics Engineering, Niigata Institute of Technology, Kashiwazaki 945-1195, Japan

A full-vectorial finite-difference (FD) scheme is proposed in this work to accurately extract the propagating modes on a magnetically biased graphene microstrip. Initially, the anisotropic surface conductivity of graphene is introduced, and the appropriate eigenvalue problem is formulated starting from Maxwell's equations. In particular, an FD approximation is utilized, while the discretization of the computation domain is based on the popular Yee cell. Then, the relationship between tangential, to the propagation direction, electromagnetic components is derived, leading to a linear eigenvalue problem. The numerical results highlight the expected difference between the propagation properties of the edge modes, thus validating the successful implementation of the featured modal solver. Moreover, it is shown that the number of unknown components is efficiently reduced due to the proper elimination of the longitudinal fields and the linearity of Maxwell's equations.

Index Terms— **Computational methods, dispersion diagram, graphene, magnetic anisotropy, sparse matrices, surface waves.**

I. Introduction

WAVEGUIDING systems based on graphene are able to facilitate long-range propagation at the far-infrared regime [1]. This is possible due to the strongly confined surface plasmon polariton (SPP) waves that are supported onto this truly 2-D carbon allotrope [2]. Thus, simple graphene waveguiding systems, such as microstrips, have been examined thoroughly, indicating the support of an infinite number of propagating modes [3]. Two major categories are identified, that is, the edge and the bulk modes, where the former exhibit increased confinement due to the respective electron concentration at the microstrip edges. Also, the application of a magnetostatic bias field, normal to the graphene microstrip, initiates even more complex phenomena because of the extra Lorentz forces imposed on electrons [4].

Hence, the development of efficient, in terms of computational resources, modal solvers is imperative for the accurate surface wave characterization of magnetically biased graphene microstrips. The attributes of the supported modes are extracted through the finite-element method (FEM) which solves the quadratic eigenvalue problem retrieved from the Helmholtz equation [5]–[7]. Although this is a powerful approach, its quadratic nature doubles the required unknown quantities during the linearization process. Therefore, linear eigenvalue problems have been established, utilizing Maxwell's equations and finite-difference (FD) schemes both for isotropic [8] and anisotropic [9] media. Herein, the domain is discretized into a Yee-cell manner for the approximation of differential equations via appropriately defined FDs. An extra merit of this concept over the FEM is its direct incorporation into the FD time-domain (FDTD) technique for full-wave simulations due to the rectangular-grid similarity.

In this article, we propose a modal solver for magnetically biased graphene waveguides stemming from Maxwell's equations. The applied FD scheme results in the prior eigenvalue problem, where only the tangential, to the waveguide cross section, components are required; thus, the number of unknown quantities is considerably decreased. The suggested method is employed for the accurate mode extraction on a realistic setup, namely a magnetically biased graphene microstrip. Numerical results indicate a deviation between the propagation properties of the edge modes as the applied magnetostatic field increases. This fact proves the validity of the proposed scheme, as the strong Lorentz forces guide electrons toward a specific edge, augmenting the concentration of the electric field.

Manuscript received 7 February 2022; revised 14 April 2022; accepted 11 May 2022. Date of publication 17 May 2022; date of current version 26 August 2022. Corresponding author: S. Amanatiadis (e-mail: samanati@auth.gr).

Color versions of one or more figures in this article are available at https://doi.org/10.1109/TMAG.2022.3175808.

Digital Object Identifier 10.1109/TMAG.2022.3175808

II. Theoretical Aspects

A. Graphene Conductivity and Surface Waves

In our work, graphene is considered as a 2-D material on the xz-plane at the far-infrared regime, while both electrostatic (corresponding to the chemical potential μ_c) and magnetostatic, B_0, biases are applied. Consequently, graphene can be characterized by its dyadic surface conductivity [10]

$$\bar{\bar{\sigma}}_{\mathrm{gr}}(\omega) = \begin{bmatrix} \sigma_{xx}(\omega) & 0 & \sigma_{xz}(\omega) \\ 0 & 0 & 0 \\ \sigma_{zx}(\omega) & 0 & \sigma_{zz}(\omega) \end{bmatrix} \tag{1}$$

where the individual elements are calculated through

$$\sigma_{xx}(\omega) = \sigma_{zz}(\omega) = \sigma_d(\omega) = \sigma_c \frac{j\omega + 2\Gamma}{\omega_c^2 + (j\omega + 2\Gamma)^2} \tag{2a}$$

$$\sigma_{xz}(\omega) = -\sigma_{zx}(\omega) = \sigma_o(\omega) = \sigma_c \frac{\omega_c}{\omega_c^2 + (j\omega + 2\Gamma)^2} \tag{2b}$$

with σ_c being the frequency-independent term

$$\sigma_c = \frac{q_e^2}{\pi \hbar^2 \Gamma} k_B T \ln\left(2\cosh\frac{\mu_c}{2k_B T}\right) \tag{3}$$

where Γ is the scattering rate, $\omega_c = q_e B_0 u_F^2/|\mu_c|$ is the cyclotron frequency, determined by the bias fields, T is the temperature, q_e is the electron charge, u_F is the Fermi velocity, and $\hbar$ and k_B are the Planck and Boltzmann constants, respectively.

The propagation attributes of the supported surface waves on graphene are strongly dependent on its surface conductivity. Explicitly, the propagation constant k_ρ of the dominant transverse magnetic (TM) term is derived via the solution of [10]

$$k_\rho = \left[\frac{1}{\eta_0^2 \sigma_d^2}\left(js^2 + \sqrt{\eta_0^2\sigma_d^2 - s^4}\right)^2 + 1\right] k_0 \tag{4}$$

with $s^2 = (\eta_0\sigma_d)^2/4 + (\eta_0\sigma_o)^2/4 + 1$ and $\eta_0 = (\mu_0/\varepsilon_0)^{1/2}$ the free-space wave-impedance.

B. FD Formulation for Modal Analysis

The featured modal solver considers a uniform waveguiding system toward the propagation direction that is valid for the majority of modern applications. In this manner, the problem is simplified significantly, since only a normal cross section is required. The analysis is based on Maxwell's equations, where graphene contribution is imported as the equivalent surface current $\vec{\mathbf{J}}_{\rm gr} = \bar{\bar{\sigma}}_{\rm gr}\vec{\mathbf{E}}$ in Ampère's law, that is,

$$\nabla \times \vec{\mathbf{E}} = -j\omega\mu_0\vec{\mathbf{H}}, \quad \nabla \times \vec{\mathbf{H}} = j\omega\varepsilon_r\varepsilon_0\vec{\mathbf{E}} + \vec{\mathbf{J}}_{\rm gr}. \tag{5}$$

Also, propagation is assumed toward the z-axis with a $e^{-j\gamma z}$ dependence for all components, where γ is the complex propagation constant of the waveguide. Note that the electric components are appropriately scaled by the free-space wave-impedance η_0 to ensure the balancing between the fields. Then, every individual component of (5) is computed through

$$-jk_0 H_x = \frac{\partial E_z}{\partial y} + j\gamma E_y \tag{6a}$$

$$-jk_0 H_y = -j\gamma E_x - \frac{\partial E_z}{\partial x} \tag{6b}$$

$$-jk_0 H_z = \frac{\partial E_y}{\partial x} - \frac{\partial E_x}{\partial y} \tag{6c}$$

$$jk_0\varepsilon_r E_x + \eta_0(J_{xx} + J_{xz}) = \frac{\partial H_z}{\partial y} + j\gamma H_y \tag{7a}$$

$$jk_0\varepsilon_r E_y = -j\gamma H_x - \frac{\partial H_z}{\partial x} \tag{7b}$$

$$jk_0\varepsilon_r E_z + \eta_0(J_{zx} + J_{zz}) = \frac{\partial H_y}{\partial x} - \frac{\partial H_x}{\partial y}. \tag{7c}$$

Herein, partial derivatives are approximated via an FD scheme at a computational domain with 2-D Yee cells, as in Fig. 1. Although a non-grid-aligned graphene layer can still be modeled via the staircase approximation, in this article, we deal with a material aligned at the xz-plane. Thus, we derive

$$-jk_0 H_x(i,j) = \frac{E_z(i,j+1) - E_z(i,j)}{\Delta y} + j\gamma E_y(i,j) \tag{8a}$$

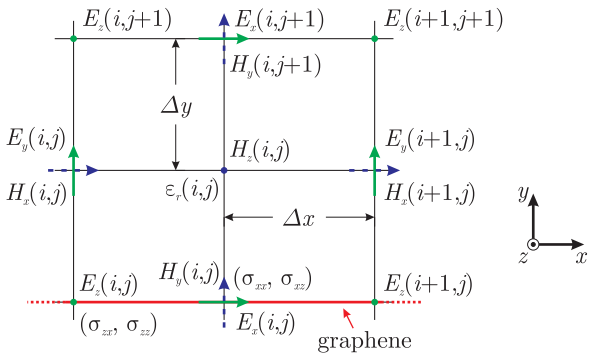

Fig. 1. Two-dimensional Yee cell including the graphene layer (in red color).

$$-jk_0 H_y(i,j) = -j\gamma E_x(i,j) - \frac{E_z(i+1,j) - E_z(i,j)}{\Delta x} \tag{8b}$$

$$-jk_0 H_z(i,j) = \frac{E_y(i+1,j) - E_y(i,j)}{\Delta x} - \frac{E_x(i,j+1) - E_y(i,j)}{\Delta y} \tag{8c}$$

$$jk_0\varepsilon_r E_x(i,j) + \frac{\eta_0}{\Delta y}\left[\sigma_d E_x(i,j) + \sigma_o E_z(i,j)\right] = \frac{H_z(i,j) - H_z(i,j-1)}{\Delta y} + j\gamma H_y(i,j) \tag{9a}$$

$$jk_0\varepsilon_r E_y(i,j) = -j\gamma H_x(i,j) - \frac{H_z(i,j) - H_z(i-1,j)}{\Delta x} \tag{9b}$$

$$jk_0\varepsilon_r E_z(i,j) + \frac{\eta_0}{\Delta y}\left[\sigma_d E_z(i,j) - \sigma_o E_x(i,j)\right] = \frac{H_y(i,j) - H_y(i-1,j)}{\Delta x} - \frac{H_x(i,j) - H_x(i,j-1)}{\Delta y}. \tag{9c}$$

It is stressed that the equivalent surface current components have been normalized to the perpendicular cell size, Δy, to enable the graphene 2-D nature. Note that $E_x(i,j)$ and $E_z(i,j)$ in (9a) and (9c) are not collocated; hence, a proper averaging is applied via the adjacent components. Also, we intend to acquire the propagation properties in terms of the $n_{\rm eff} = \gamma/k_0$ effective index, that is, the ratio between the mode propagation constant γ to the free-space wavenumber k_0. The effective index provides an intuitive waveguide perception because of its direct comparison to the free-space wavenumber. Specifically, $n_{\rm eff}$ values larger than 1 lead to slower waves with a smaller wavelength compared to free-space propagation. To this end, (8) and (9) are written in the compact matrix form of

$$-j\begin{bmatrix}\mathbf{H}_x\\ \mathbf{H}_y\\ \mathbf{H}_z\end{bmatrix} = \begin{bmatrix}\mathbf{0} & jn_{\rm eff}\mathbf{I} & \mathbf{U}_y\\ -jn_{\rm eff}\mathbf{I} & \mathbf{0} & -\mathbf{U}_x\\ -\mathbf{U}_y & \mathbf{U}_x & \mathbf{0}\end{bmatrix}\begin{bmatrix}\mathbf{E}_x\\ \mathbf{E}_y\\ \mathbf{E}_z\end{bmatrix} \tag{10}$$

$$\left(j\begin{bmatrix}\boldsymbol{\varepsilon}_r & \mathbf{0} & \mathbf{0}\\ \mathbf{0} & \boldsymbol{\varepsilon}_r & \mathbf{0}\\ \mathbf{0} & \mathbf{0} & \boldsymbol{\varepsilon}_r\end{bmatrix} + \frac{1}{\omega\varepsilon_0\Delta y}\begin{bmatrix}\boldsymbol{\sigma}_d & \mathbf{0} & \boldsymbol{\sigma}_o\\ \mathbf{0} & \mathbf{0} & \mathbf{0}\\ -\boldsymbol{\sigma}_o & \mathbf{0} & \boldsymbol{\sigma}_d\end{bmatrix}\right)\begin{bmatrix}\mathbf{E}_x\\ \mathbf{E}_y\\ \mathbf{E}_z\end{bmatrix} = \begin{bmatrix}\mathbf{0} & jn_{\rm eff}\mathbf{I} & \mathbf{V}_y\\ -jn_{\rm eff}\mathbf{I} & \mathbf{0} & -\mathbf{V}_x\\ -\mathbf{V}_y & \mathbf{V}_x & \mathbf{0}\end{bmatrix}\begin{bmatrix}\mathbf{H}_x\\ \mathbf{H}_y\\ \mathbf{H}_z\end{bmatrix} \tag{11}$$

where $\mathbf{I}$ is a square identity matrix and $\boldsymbol{\varepsilon}_r$ a diagonal matrix corresponding to the relative permittivity of each cell.

Also, $\mathbf{U}_x$, $\mathbf{U}_y$, $\mathbf{V}_x$, and $\mathbf{V}_y$ are sparse square matrices determined by means of the finite differentiation and the boundary conditions. The form of these matrices depends on the numbering of the unknown components in the computational grid and in the case of a sequential order, $\mathbf{U}_x$ is given by

$$\mathbf{U}_x = \frac{1}{k_0 \Delta x} \begin{bmatrix} 1 & & & & \\ -1 & 1 & & & \\ & \ddots & \ddots & & \\ & & & -1 & 1 \\ & & & & -1 \end{bmatrix} \tag{12}$$

with similar expressions holding for the other matrices. Evidently, the set of equations for the longitudinal components, for example, E_z and H_z, does not involve n_{eff}. So, they can be eliminated by replacing them with their tangential counterparts. This process is, also, possible before the FD approximation and other discretization schemes, such as the FE, are applied via an entirely different formulation. However, the featured FD method exploits the arrangement of components at the Yee cell to retain the rationale of partial derivatives in Maxwell's equations. Then, some matrix manipulations are conducted in (10) and (11) to eliminate the longitudinal components, as mentioned above, and solve for n_{eff}. In this context, our eigenvalue problem receives the linear matrix form of

$$\left(\begin{bmatrix} \mathbf{A}_{xx}^{ee} & \mathbf{0} & \mathbf{A}_{xx}^{em} & \mathbf{A}_{xy}^{em} \\ \mathbf{A}_{yx}^{ee} & \mathbf{0} & \mathbf{A}_{yx}^{em} & \mathbf{A}_{yy}^{em} \\ \mathbf{A}_{xx}^{me} & \mathbf{A}_{xy}^{me} & \mathbf{0} & \mathbf{0} \\ \mathbf{A}_{yx}^{me} & \mathbf{A}_{yy}^{me} & \mathbf{A}_{yx}^{mm} & \mathbf{A}_{yy}^{mm} \end{bmatrix} - n_{\text{eff}} \mathbf{I} \right) \begin{bmatrix} \mathbf{E}_x \\ \mathbf{E}_y \\ \mathbf{H}_x \\ \mathbf{H}_y \end{bmatrix} = \mathbf{0}. \tag{13}$$

Here, $\mathbf{A}_{\{\dots\}}^{\{\dots\}}$ are, also, sparse matrices that refer to the relationship between the tangential, to the propagation, electromagnetic components and they are extracted as

$$\mathbf{A}_{xx}^{ee} = -j\mathbf{U}_x \left(j\boldsymbol{\varepsilon}_r + \frac{\boldsymbol{\sigma}_d}{\omega\varepsilon_0 \Delta y} \right)^{-1} \frac{\boldsymbol{\sigma}_o}{\omega\varepsilon_0 \Delta y}$$

$$\mathbf{A}_{xx}^{em} = -j\mathbf{U}_x \left(j\boldsymbol{\varepsilon}_r + \frac{\boldsymbol{\sigma}_d}{\omega\varepsilon_0 \Delta y} \right)^{-1} \mathbf{V}_y$$

$$\mathbf{A}_{xy}^{em} = j\mathbf{U}_x \left(j\boldsymbol{\varepsilon}_r + \frac{\boldsymbol{\sigma}_d}{\omega\varepsilon_0 \Delta y} \right)^{-1} \mathbf{V}_x + \mathbf{I}$$

$$\mathbf{A}_{yx}^{ee} = -j\mathbf{U}_y \left(j\boldsymbol{\varepsilon}_r + \frac{\boldsymbol{\sigma}_d}{\omega\varepsilon_0 \Delta y} \right)^{-1} \frac{\boldsymbol{\sigma}_o}{\omega\varepsilon_0 \Delta y}$$

$$\mathbf{A}_{yx}^{em} = -j\mathbf{U}_y \left(j\boldsymbol{\varepsilon}_r + \frac{\boldsymbol{\sigma}_d}{\omega\varepsilon_0 \Delta y} \right)^{-1} \mathbf{V}_y - \mathbf{I}$$

$$\mathbf{A}_{yy}^{em} = j\mathbf{U}_y \left(j\boldsymbol{\varepsilon}_r + \frac{\boldsymbol{\sigma}_d}{\omega\varepsilon_0 \Delta y} \right)^{-1} \mathbf{V}_x$$

$$\mathbf{A}_{xx}^{me} = \mathbf{V}_x \mathbf{U}_y$$

$$\mathbf{A}_{xy}^{me} = j\boldsymbol{\varepsilon}_r - \mathbf{V}_x \mathbf{U}_x$$

$$\mathbf{A}_{yx}^{me} = -j\boldsymbol{\varepsilon}_r + \mathbf{V}_y \mathbf{U}_y + j \frac{\boldsymbol{\sigma}_o}{(\omega\varepsilon_0 \Delta y)^2} \left(j\boldsymbol{\varepsilon}_r + \frac{\boldsymbol{\sigma}_d}{\omega\varepsilon_0 \Delta y} \right)^{-1} \boldsymbol{\sigma}_o$$

$$\mathbf{A}_{yy}^{me} = -\mathbf{V}_y \mathbf{U}_x$$

$$\mathbf{A}_{yx}^{mm} = j \frac{\boldsymbol{\sigma}_o}{\omega\varepsilon_0 \Delta y} \left(j\boldsymbol{\varepsilon}_r + \frac{\boldsymbol{\sigma}_d}{\omega\varepsilon_0 \Delta y} \right)^{-1} \mathbf{V}_y$$

$$\mathbf{A}_{yy}^{mm} = -j \frac{\boldsymbol{\sigma}_o}{\omega\varepsilon_0 \Delta y} \left(j\boldsymbol{\varepsilon}_r + \frac{\boldsymbol{\sigma}_d}{\omega\varepsilon_0 \Delta y} \right)^{-1} \mathbf{V}_x.$$

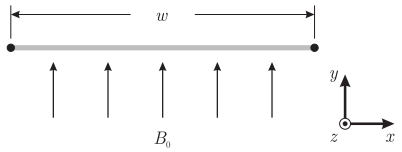

Fig. 2. Graphene plasmonic waveguide that consists of a w-wide microstrip and a perpendicular, to its surface, magnetostatic bias B_0.

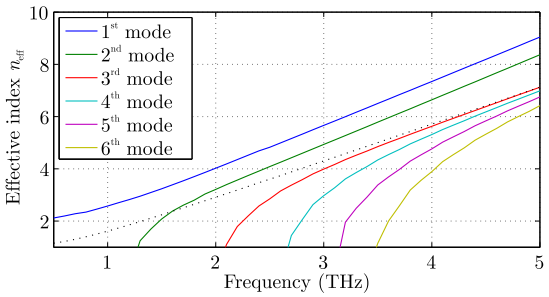

Fig. 3. Dispersion curves for a free-standing 40 μm-wide graphene layer with $\Gamma = 0.11$ meV, $\mu_c = 0.2$ eV, and $B_0 = 0.5$ T. The black dotted line corresponds to the propagation on a sheet with infinite dimensions.

It is stressed that parallel components have been efficiently eliminated by the proposed FD scheme, thus reducing notably the number of unknown coefficients. Finally, the computational domain is terminated by an eight-cell perfectly matched layer (PML) to annihilate artificial reflected waves [9].

III. Numerical Validation

To verify our solver, we examine the magnetically biased free-standing 40 μm-wide graphene strip of Fig. 2. Its parameters are $\mu_c = 0.2$ eV and $\Gamma = 0.11$ meV at temperature $T = 300$ K, while $B_0 = 0.5$ T with its direction normal to graphene. Our analysis is performed at the 0.5–5 THz range and the domain is 300 μm $\times$ 200 μm. The unit cells on graphene and its vicinity are chosen much smaller than the free-space wavelength λ_0 to model precisely the rapid fluctuations of surface waves. So, Δx and Δy are set to $\lambda_0/400$ at each evaluation frequency.

The dispersion curves of various propagating modes are given in Fig. 3. Interestingly, there is not any cut-off frequency for the first mode, indicating a surface wave propagation at the entire spectrum. The second mode appears at around 1.25 THz, whereas the remaining ones propagate effectively beyond 2 THz. Note that the first two modes degenerate into edge ones and present a constant difference in their effective indices. All the other modes, identified as bulk ones, concentrate at the microstrip body and converge to the infinite layer propagation properties, calculated via (4), at higher frequencies.

The electric field distribution is displayed in Fig. 4. Here, the concentration at the left edge, the first mode, is remarkably increased compared to the right edge, the second mode, since the electric field amplitude is almost doubled. This is expected, as the Lorentz forces on electrons, due to the magnetostatic bias, predict a higher field concentration at a specific edge. Thus, surface wave phenomena are more intense at this edge, explaining the prior constant difference between the effective indices of the edge modes. For the bulk modes, that is, the

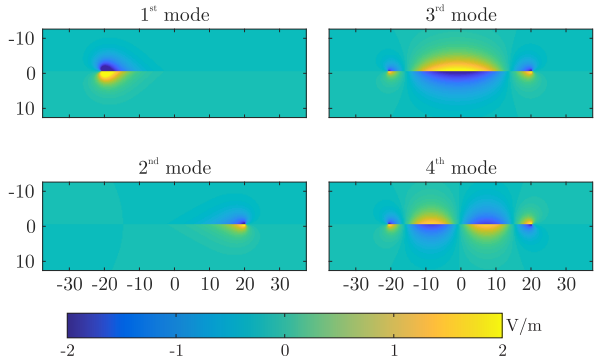

Fig. 4. Distribution of the electric field component that is normal to a free-standing 40 μm-wide graphene layer with $\Gamma = 0.11$ meV, $\mu_c = 0.2$ eV, and $B_0 = 0.5$ T at 3 THz. The colorbar limits are identical for all modes.

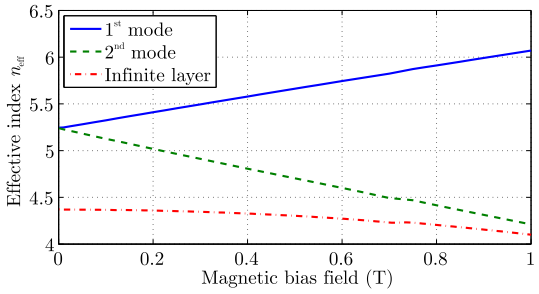

Fig. 5. Effective index variation of the edge modes on a 40 μm-wide graphene microstrip versus the magnetostatic bias field at 3 THz.

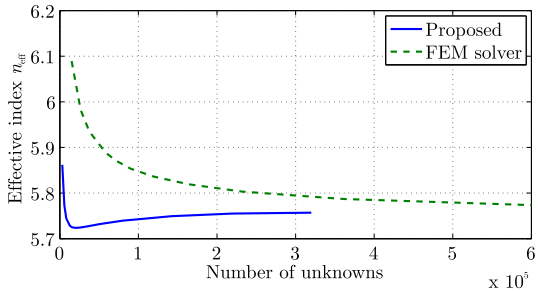

Fig. 6. Convergence of the proposed modal solver compared to a conventional FEM one in terms of the required number of unknown components.

third, fourth, and so on, the electric field concentrates at the microstrip main body, while oscillations increase with the mode order.

Next, the influence of the magnetostatic bias on the edge modes is studied in Fig. 5. The frequency is constant at 3 THz and the variation of B_0 reveals that the n_{eff} difference between the edge modes augments for stronger fields. In particular, the two modes propagate identically in the absence of B_0, yet their difference is almost 33% for $B_0 = 1$ T. Indeed, the Lorentz forces drive the electrons to the left edge, while the right one approximates the infinite layer propagation, as derived via (4).

Finally, the efficiency of our algorithm versus the eigenvalue problem complexity is compared to a typical FEM modal solver [7]. The first mode of the graphene microstrip waveguide is analyzed using different discretization levels. As the mesh becomes denser, we expect that the solution converges, yet the number of unknowns increases. Indeed, Fig. 6 indicates that a relatively coarse mesh (less than 100 000 unknowns) is not adequate for both solvers, as the error is over 1%. The featured scheme converges to the correct n_{eff} value for about 310 000 unknowns; almost half compared to the FEM solver. This is, mainly, due to the linearity of the eigenvalue problem and the elimination of the normal, to the cross section, components. Regarding time consumption, the Arnoldi process is used for both solvers and the required time is equivalent (less than 10% deviation) for matrices of the same size.

IV. Conclusion

A Maxwellian-oriented linear eigenvalue solver has been introduced in this work for the accurate mode extraction of magnetically biased graphene waveguides. The fundamental differential equations are approximated by an FD scheme, which discretizes the computational domain in a Yee-cell fashion. The validity of our algorithm has been successfully proved via the popular graphene microstrip setup since the expected propagation difference between the edge modes emerged. Lastly, the efficiency of the proposed technique, with regard to the necessary unknown variables, has been highlighted because of its linear nature and the necessity of exclusively tangential, to the waveguide cross section, electromagnetic components.

Acknowledgment

This work was supported in part by Greece and the European Union [European Social Fund (ESF)] through the Operational Program (Human resources development, education and lifelong learning) in the context of the project "Reinforcement of Postdoctoral Researchers-2nd Cycle," implemented by the State Scholarships Foundation (IKY) under Grant MIS-5033021.

References

[1] M. U. Shahid, A. Ghaffar, M. A. S. Alkanhal, and Y. Khan, "Propagation of electromagnetic waves in graphene-wrapped cylindrical waveguides filled with magnetized plasma," *Optik*, vol. 244, Oct. 2021, Art. no. 167566.

[2] Y. V. Bludov, A. Ferreira, N. M. Peres, and M. I. Vasilevskiy, "A primer on surface plasmon-polaritons in graphene," *Int. J. Mod. Phys. B*, vol. 27, no. 10, Apr. 2013, Art. no. 1341001.

[3] A. Y. Nikitin, F. Guinea, F. J. García-Vidal, and L. Martín-Moreno, "Edge and waveguide terahertz surface plasmon modes in graphene microribbons," *Phys. Rev. B, Condens. Matter*, vol. 84, no. 16, 2011, Art. no. 161407.

[4] D. L. Sounas and C. Caloz, "Gyrotropy and nonreciprocity of graphene for microwave applications," *IEEE Trans. Microw. Theory Techn.*, vol. 60, no. 4, pp. 901–914, Apr. 2012.

[5] S. Selleri, L. Vincetti, A. Cucinotta, and M. Zoboli, "Complex FEM modal solver of optical waveguides with PML boundary conditions," *Opt. Quant. Electron.*, vol. 33, nos. 4–5, pp. 359–371, Apr. 2001.

[6] I. Demirtzioglou and T. Yioultsis, "Analysis of graphene plasmonic waveguides and switching components via a finite element formulation with surface conductivity," *PIERS Proc.*, pp. 2352–2356, Jul. 2015.

[7] V. Salonikios, S. Amanatiadis, N. Kantartzis, and T. Yioultsis, "Modal analysis of graphene microtubes utilizing a two-dimensional vectorial finite element method," *Appl. Phys. A, Solids Surf.*, vol. 122, no. 4, pp. 1–7, Apr. 2016.

[8] Z. Zhu and T. G. Brown, "Full-vectorial finite-difference analysis of microstructured optical fibers," *Opt. Exp.*, vol. 10, pp. 853–864, Aug. 2002.

[9] M.-Y. Chen, S.-M. Hsu, and H.-C. Chang, "A finite-difference frequency-domain method for full-vectorial mode solutions of anisotropic optical waveguides with an arbitrary permittivity tensor," *Opt. Exp.*, vol. 17, no. 8, pp. 5965–5979, 2009.

[10] G. W. Hanson, "Dyadic Green's functions for an anisotropic, non-local model of biased graphene," *IEEE Trans. Antennas Propag.*, vol. 56, no. 3, pp. 747–757, Mar. 2008.